

BoundarySqueeze: Image Segmentation as Boundary Squeezing

Hao He^{1 2 *}, Xiangtai Li^{3 5 *}, Kuiyuan Yang⁴, Guangliang Cheng⁵, Jianping Shi⁵,
Yunhai Tong³, ZhengJun Zha⁶, Lubin Weng²

¹ NLPR, Institute of Automation, Chinese Academy of Sciences

² School of Artificial Intelligence, University of Chinese Academy of Sciences

³ Key Laboratory of Machine Perception (MOE), Peking University

⁴ DeepMotion ⁵ SenseTime Research ⁶ USTC

ABSTRACT

We propose a novel method for fine-grained high-quality image segmentation of both objects and scenes. Inspired by dilation and erosion from morphological image processing techniques, we treat the pixel level segmentation problems as squeezing object boundary. From this perspective, we propose **Boundary Squeeze** module: a novel and efficient module that squeezes the object boundary from both inner and outer directions which leads to precise mask representation. To generate such squeezed representation, we propose a new bidirectionally flow-based warping process and design specific loss signals to supervise the learning process. Boundary Squeeze Module can be easily applied to both instance and semantic segmentation tasks as a plug-and-play module by building on top of existing models. We show that our simple yet effective design can lead to high qualitative results on several different datasets and we also provide several different metrics on boundary to prove the effectiveness over previous work. Moreover, the proposed module is light-weighted and thus has potential for practical usage. Our method yields large gains on COCO, Cityscapes, for both instance and semantic segmentation and outperforms previous state-of-the-art PointRender in both accuracy and speed under the same setting. Code and model will be available.

1 INTRODUCTION

Image segmentation tasks comprehensively understand image content by densely predicting binary masks for each object (instance segmentation) or each category (semantic segmentation) [10, 27, 47]. As for humans, image segmentation is precisely annotated in another paradigm, where the efforts are focused on mask boundaries. In this paper, we aim to improve image segmentation by also emphasizing precise localization of mask boundaries as human labeling.

Recent state-of-the-art works for both instance segmentation and semantic segmentation are based on fully convolution network (FCN) [11, 27, 38, 47, 78]. With FCN, features are densely generated on a spatial grid, where mask predictions are accomplished by classifying features in a Region of Interest (RoI) or whole image. These methods treat all pixels equally, and ignore the challenge of generating discriminative features for boundary pixels. Accordingly, non-uniform representations [15, 38] are proposed to process boundary pixels in a special way. Boundary-Preserving Mask R-CNN [15] adds a boundary branch to refine the mask, while PointRender [38] adaptively selects a non-uniform set of points to refine during the upsampling process.

* The first two authors contribute equally to this work. The code will be available at <https://github.com/lxtGH/BSeg>.

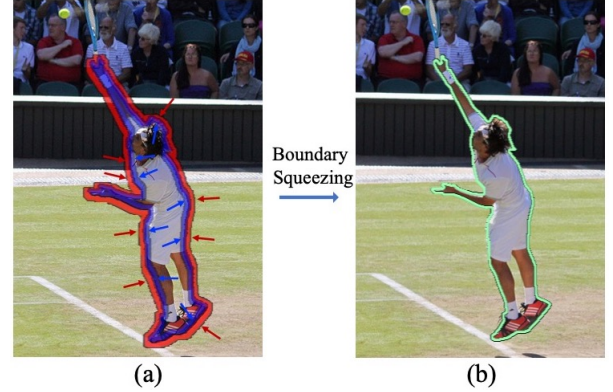


Figure 1: Illustration of the boundary squeezing process. In (a), the red arrows mean squeeze boundary features from the object’s outside (contraction process), while the blue arrows mean squeeze boundary features from inside of the object (expansion process). These two processes complement each other and help generate accurate boundary (green line in (b)). Best viewed on screen and zoom in.

However, both works have several shortcomings. For the former, directly learning the object boundaries is hard. For the latter, point-based sampling and rendering along the boundary can not guarantee the structural failure case of objects. As shown in the first row of Fig. 2, the baseball bat has a similar appearance to the background wall. The rendering module in PointRender fails to classify the background and foreground things since there is no boundary bound and the points for rendering are sampled from coarse features without guidance.

As mentioned previously, in this work, we want to unify the two different segmentation problems via boundary bound. We propose a conceptually new approach named Boundary Squeeze for modeling segmentation representation. Our insight is squeezing the object boundary from two different directions, leading to a much finer boundary feature representation. The illustration is shown in Fig. 1. Such precise boundary feature representation benefits the segmentation tasks and achieves significant improvement on mask quality. Compared with the previous rendering based [38], our method can preserve more structural information and avoid the shortcomings of randomly selected points. The segmentation results of our method are shown in the third and fifth columns of Fig. 2.

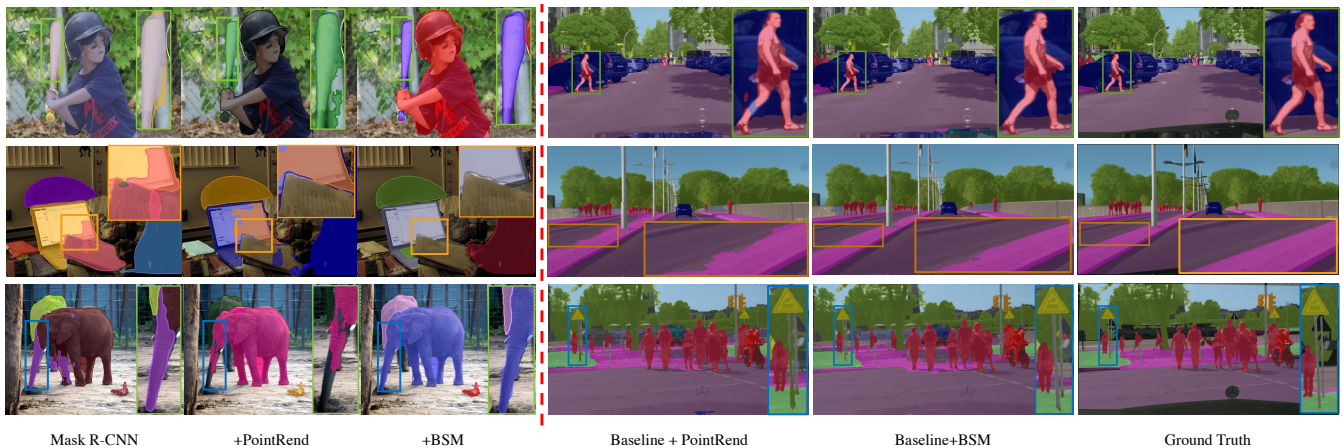


Figure 2: Example result pairs: (a) Left: from Mask R-CNN [27] vs. PointRender [38] and vs. Our Boundary Squeeze, using ResNet-50 [29] backbone. (b) Right: from DeeplabV3+ [11] PointRender [38] vs. Our Boundary Squeeze. Note that our model predicts masks with more structural object boundaries where the PointRender fails to predict the finer details.

Our approach is inspired by the previous traditional binary segmentation, such as differential edge detection and morphological processing [22, 51]. Our approach has two opposite directions to squeeze the boundary: one from outer parts and the other from the inner parts. We design a novel flow-based warping module to let the network learn to achieve these purposes. In particular, there are two independent modules supervised by two different mask labels. One is the dilation (or contraction) results of original masks, while the other is erosion (or expansion) results of original masks. The dual supervisions from both maps work complementary and result in much more satisfactory boundary results. We term our new network module as the **Boundary Squeeze** module.

Our Boundary Squeeze is a general module that allows many implementations on different frameworks. It can be a plug-in module for the current state-of-the-art network to refine object boundary in an end-to-end manner. For example, it can be appended into Mask R-CNN-like network [4, 27] by replacing the mask head with our proposed Boundary Squeeze mask head for instance segmentation task. It can also be appended at the end of modern semantic segmentation networks such as DeeplabV3+ [11] for refining the semantic segmentation. These will be detailed in the latter section.

We evaluate our Boundary Squeeze on the instance and semantic segmentation tasks using COCO [44], Cityscapes [16], BDD [72] benchmarks. From qualitative results, our module outputs sharp and more structural boundaries, which are better than recent state-of-the-art PointRender [38] as illustrated in Fig. 2. We also observe quantitative improvements over the PointRender through various metrics, including standard intersection-over-union based metrics for these tasks (mask AP and mIoU). Since these metrics are biased towards object-interior pixels and are relatively insensitive to boundary improvements [14], we also compute the boundary-aware metrics (F-score and recent proposed boundary AP [14]). Our method also achieves improvement over PointRender under the same setting [67] while running more efficiently. These results prove the effectiveness of our Boundary Squeeze. To summarize, our contributions have the following aspects:

- We propose Boundary Squeeze, a novel and efficient module by treating the segmentation as boundary squeezing process. The module is supervised via different labels, which can be obtained from mask annotation for free.
- Boundary Squeeze can be performed as a plug-and-play module by easily being deployed into current state-of-the-art segmentation methods, including Mask R-CNN [27] and DeeplabV3+ [11]. Extensive experiments and analysis have verified the effectiveness of the proposed method.
- Our approach can produce finer boundary results. It has more structural outputs than PointRender [38]. We achieve better results than PointRender and Boundary-Preserving Mask R-CNN [15] over different metrics on COCO [44] and Cityscapes datasets while running more efficiently.
- The proposed approach is also verified for the semantic segmentation task on Cityscapes [16] and BDD [72] datasets. It also improves strong DeeplabV3+ models [11] by a significant margin.

2 RELATED WORK

In this section, we will review the related work in three different aspects: boundary processing, instance segmentation and semantic segmentation.

Boundary Processing: Modeling boundary has a long history in computer vision community. Boundary detection has been a fundamental computer vision task as it provides an essential cue for recognition. In the era of deep learning, some CNN-based methods have significantly pushed the development of this field, such as [20, 28, 39, 48, 57, 71]. Snake [34] and Deep Snake [53] refine the initial object contours recursively through specific operations such as circular convolution. CASENet [74] proposes a challenging task of category-aware boundary detection. InstanceCut [37] adopts boundaries to partition semantic segmentation into instance-level segmentation. Different from previous works, our methods treat object segmentation as a boundary squeezing process where the

boundary of the segmentation mask is squeezed into a thinner representation via specific supervisions.

Instance Segmentation: Instance Segmentation aims to detect and segment each instance [17, 26]. The two-stage pipeline Mask R-CNN and its variants [4, 7, 27, 30, 58, 66] first generate object proposals using Region Proposal Network (RPN) [55] and then predict boxes and masks on each RoI feature. Further improvements have been made to boost its accuracy. PANet [45] introduces bottom-up path to enrich FPN features, and Mask Scoring R-CNN [30] addresses the misalignment between the confidence score and localization accuracy of predicted masks. HTC [7] extends the Cascade Mask R-CNN [4] by augmenting a semantic segmentation branch. SCNet [61] balances the IoU distribution of the samples for both training and inference. Several single-stage methods [3, 6, 12, 60, 63, 64, 69, 77] achieve significant progress and comparable results with two-stage pipelines. Meanwhile, there are several bottom-up approaches [19, 46, 50]. Accurate boundary localization can explicitly contribute to the mask prediction for instance segmentation, and there are many recent work [13, 15, 38] focus on boundary modeling. In particular, PointRend [38] handles the image segmentation upsampling procedure as a rendering process via a shared multiple-layer network. Boundary preserving Mask R-CNN [15] proposes to predict instance-level boundaries to augment the mask head. Although those work achieves better segmentation results, the extra computation results in slow inference speed which will be shown in experiment section. Rather than direct fusing edge information into mask head, our method treats the instance segmentation as a boundary squeezing process and can fully utilize the limited mask annotation.

Semantic Segmentation: Semantic Segmentation is required to assign a semantic label for each pixel. Fully convolutional networks (FCNs) [47] are the foundation of modern semantic segmentation approaches. Recent approaches try to overcome the limited receptive field of FCNs by multi-scale pooling [68, 78], dilated convolution [9–11, 73], non-local operators [23, 32, 41, 62, 75, 76]. There are also several works on modeling semantic segmentation boundaries [1, 2, 8, 35, 40, 59]. Previous works obtain better boundary localization by structure modeling, such as boundary neural fields [1], affinity field [35], random walk [2]. The work [8, 24] adopts edge information to refine network output by predicting edge maps from intermediate CNN layers. Zhu et al. [82] uses boundary relation loss to utilize coarse predicted segmentation labels for data augmentation. Gated-SCNN [59] adds a boundary stream to learn detailed low-level information by gated convolution. Our method can be a plug-in method and can be easily extended into semantic segmentation methods. We show our method can improve the state-of-the-art semantic segmentation method on different datasets.

3 METHOD

Overview: In this section, we will first describe the motivation of our approach. Then we will introduce some notations of our method. After that, the details of our Boundary Squeeze Module will be presented. In particular, we take instance segmentation setting for the illustration. Then the supervision signals of our method will be presented. Finally, we will describe how to deploy

our module on two segmentation tasks: instance segmentation and semantic segmentation.

3.1 Boundary Squeeze Module (BSM)

Motivation: As mentioned in the previous section, our method is inspired by traditional morphological processing [22, 51]. The boundary squeezing process is the simulation of the dilation and erosion processes via a learned neural network. Rather than regular processing of the binary image, we process the feature map, which makes the entire process into an end-to-end manner, and such a network can be trained in a data-driven way. The second advantage of the processing feature is that this design is general and flexible and can be applied in different segmentation tasks, such as semantic segmentation and instance segmentation.

Notation: We introduce several notations for the following sections in this part. We use the Mask R-CNN-based instance segmentation setting to illustrate our method. F_{RoI} is produced using RoIAlign [27] from P2-P5 FPN [42] features. We also use RoIAlign and P2 FPN features to produce F'_{RoI} . Note that the size of F_{RoI} is 14×14 , while the original size of F'_{RoI} is 28×28 then one 1×1 convolution layer is used to downsample the resolution of F'_{RoI} to 14×14 . We denote the features for dilation (or called **contraction**) branch as $F_{contraction}$ and the features for erosion (or called **expansion**) branch as $F_{expansion}$. The loss function for each branch is $L_{contraction}$ and $L_{expansion}$, respectively. The squeezed feature of the boundary branch is denoted as $F_{boundary}$, and the boundary branch is supervised by $L_{boundary}$. The ground truth of segmentation branch, boundary branch, contraction branch, and expansion branch are G_s , G_b , G_c , and G_e separately.

Details of Boundary Squeeze Module: As shown in Fig. 3(b), the BSM takes two distinct RoI features (F_{RoI} and F'_{RoI}) as inputs and outputs three different features, including $F_{boundary}$, $F_{contraction}$, and $F_{expansion}$. First, F_{RoI} and F'_{RoI} are added together to get F_{sum} . The choice of F'_{RoI} follows the design of the previous works [6, 11, 38], by introducing low-level and high-frequency details into the F_{RoI} , which benefits the boundary squeezing process. Then F_{sum} is fed into two parallel branches: contraction branch and expansion branch. In both branches, two 3×3 convolution layers are first used to generate its unique features F'_{sum} , after that, a Squeezed Feature Generator (SFG) is utilized to produce squeezed feature ($F_{contraction}$ or $F_{expansion}$). $F_{contraction}$ and $F_{expansion}$ are used to squeeze boundary features from the outside and inside of an object, respectively. SFG will be detailed in the following parts. Finally, both squeezed features and F_{RoI} are summed together in a residual manner [29] as the final squeezed boundary feature $F_{boundary}$, formulated as $F_{boundary} = F_{contraction} + F_{expansion} + F_{RoI}$.

Squeezed Feature Generator: We propose a flow-based approach to generate the squeezed features. The inputs of SFG are F'_{sum} and F_{RoI} , and the output is one squeezed feature i.e. $F_{contraction}$ or $F_{expansion}$. Specifically, following [21], we first concatenate F'_{sum} and F_{RoI} then adopt one 3×3 convolution layer to generate the flow field $\delta \in \mathbb{R}^{14 \times 14 \times 2}$ for each RoI. With δ , features of each position p_l on the standard spatial grid F'_{sum} are mapped to a new position \hat{p} via $p_l + \delta_l(p_l)$. We use the differentiable bilinear sampling mechanism

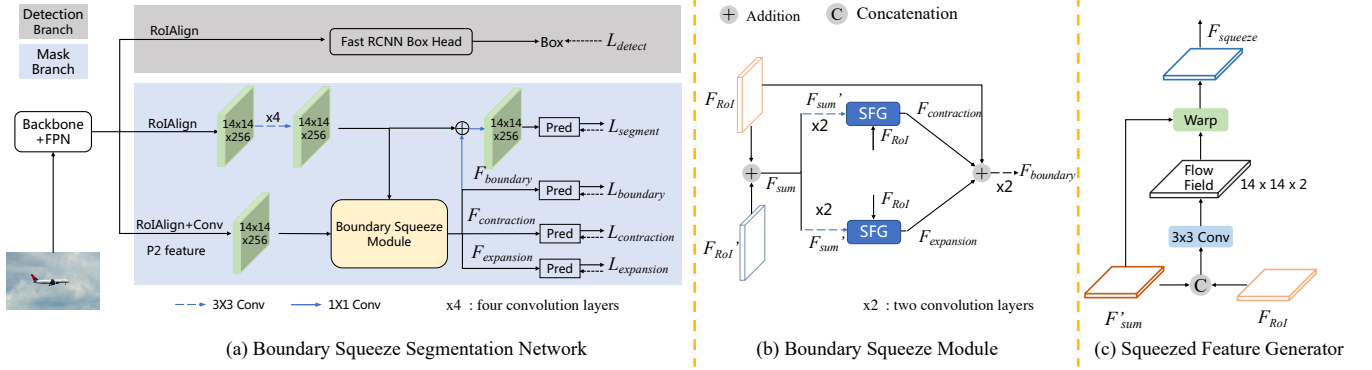


Figure 3: Network Architecture of our proposed Boundary Squeeze. (a), The entire pipeline of our Boundary Squeeze network with Mask RCNN as the example. (b), The details of our proposed Boundary Squeeze Module. SFG: Squeeze Feature Generator. (c), The details of Squeezed Feature Generator. Best view it in color and zoom in.

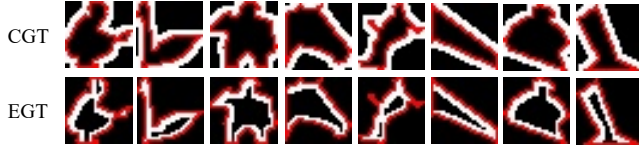


Figure 4: Visualization of Contraction branch Ground Truth (CGT) and Expansion branch Ground Truth (EGT). White pixels are positive while black pixels are negative. Boundary pixels are labeled as red to distinguish positive pixels and negative pixels.

to achieve this process. This sampling mechanism, proposed in the spatial transformer networks [33, 81], linearly interpolates the values of the four nearest neighbor pixels of p_l from F'_{sum} . This process can be formulated using Equ. 1.

$$F_{squeeze}(p_x) = \sum_{p \in N(p_l)} w_p F'_{sum}(p) \quad (1)$$

where w_p calculated from flow map δ , represents bilinear kernel weights on the warped spatial grid. N represents the number of involved neighboring pixels. The whole process of SFG is illustrated in Fig. 3 (c).

Essentially, the warping process is the deformation of the entire RoI feature, and one can also choose other methods to achieve the same purpose, like deformable convolution [18]. However, though deformable convolution results in a similar performance, it needs more inference time, which can be found in the experiment section.

Supervision Signals: The different supervision signals control the warping operation's direction of the contraction branch and expansion branch. Given a binary mask annotation G_s , we use Equ. 2 to generate G_c and G_e where $H_{dilation}$ is the dilation operation in morphological processing which can extend the G_s 's boundary into the background, and $H_{erosion}$ is the erosion operation which is used to shrink G_s from its original border. K is the kernel size of $H_{dilation}$ and $H_{erosion}$.

$$\begin{cases} G_c = H_{dilation}(G_s, K) - G_s, \\ G_e = G_s - H_{erosion}(G_s, K) \end{cases} \quad (2)$$

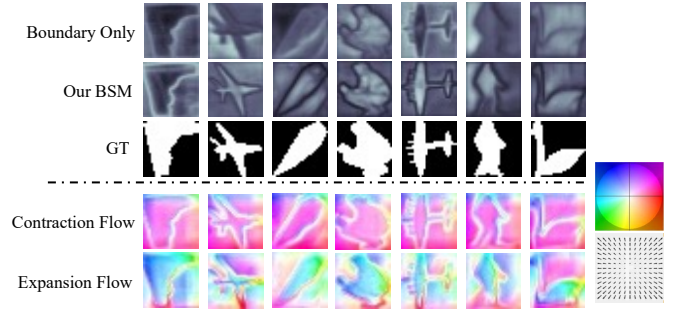


Figure 5: Visual Interpretation of Our proposed BSM. (a) The top sub-figure shows the comparison results on instance feature representation of boundary. (Boundary Only supervision and our BSM results). GT means the Ground Truth mask. Our BSM outputs thinner and more precise boundaries, and it also contains more structural information. (b) The bottom sub-figure visualizes the two types of learned flow fields. Best view it on the screen and zoom in.

The visualization of some G_c and G_e can be found in Fig. 4. Following [15], we use the Laplacian operator to generate G_b . The supervision signal of the segmentation branch is the original G_s .

Visual Interpretation: To better understand our boundary squeezing process, we present two types of visual interpretations in Fig. 5. The first is the instance-aware feature visualization and the second is the visualization of two flow fields learned from two independent branches. As shown at the top of Fig. 5, compared with directly predict boundary, like [1] does, our BSM produces a clearer and thinner boundary feature representation $F_{boundary}$. Note that we utilize Principal Component Analysis (PCA) [65] to reduce the number of $F_{boundary}$'s dimension into three for visualization. This comparison result proves our motivation: squeezed boundary feature results in a more discriminative and structural-preserving representation. The bottom parts of Fig. 5 show two different flow fields. For the contraction branch, the direction of learned flow points is to the inner parts of instance objects, while the direction of learned flow mainly expands to the outside of instance objects in the expansion branch.

Both flows squeeze the object boundary in a complementary way and benefit each other, proven in the experiment section.

3.2 Boundary Squeeze on Segmentation Task

In this section, we will describe how to deploy our proposed BSM on two segmentation tasks.

Instance Segmentation: For instance segmentation task, we adopt the Mask R-CNN [27] as the baseline method. As shown in Fig. 3(a), the proposed BSM is inserted after the four consecutive 3×3 convolution layers of Mask R-CNN head. And the final prediction head¹ (denote as Pred in Fig. 3(a)) is the same with Mask R-CNN. The kernel size of dilation and erosion operations is set to 5 and the relevant experiments can be found in supplementary. The total loss $L_{instance}$ is the combination of multi-tasks learning, formulated as $L_{instance} = L_{detection} + L_{mask}$. $L_{detection}$ is the loss of detection branch and $L_{mask} = L_{segmentation} + L_{boundary} + L_{contraction} + L_{expansion}$. $L_{segmentation}$ is Binary Cross-Entropy loss (BCE), $L_{boundary}$ is the combination of BCE and Dice loss [49], $L_{contraction}$ and $L_{expansion}$ are Dice loss. During inference, we take the output of the segmentation branch as the model’s output.

Semantic Segmentation: For the semantic segmentation task, we choose DeeplabV3+ [11] as our baseline. In particular, the proposed BSM is appended at the end of DeeplabV3+ head (after the output of Atrous Spatial Pyramid Pooling). We treat the entire feature map as one RoI in instance segmentation task. The low-level feature is the same as the DeeplabV3+ design. For supervision signal generation, since most semantic segmentation datasets [16, 72, 79] have no separate background class, to simulate the expansion and contraction process, we adopt the binary setting for each class. We treat each semantic class as one binary mask, which means each class in the semantic segmentation label map is one RoI in the instance segmentation setting. Then we can fully utilize the same setting as instance segmentation. The kernel size of dilation and erosion operations is set to 15. The entire training process is supervised by both original Cross-Entropy loss and three extra losses (boundary loss and two independent Dice losses on two squeezing branches), which are the same as the instance segmentation task.

4 EXPERIMENT

4.1 Experiment: Instance Segmentation

Overview: We first conduct experiments on the instance segmentation task. We perform extensive ablation experiments on the challenging COCO dataset [44]. We also present experimental results on the Cityscapes [16] and LVIS [25].

Dataset: (a) COCO contains 118k images for training, 5k images for validation, and 20k images for testing. Following the common practice [15, 27, 43], we train our models using the training set (*train2017*) and report results on the validation set (*val2017*) for ablation studies. We also report the results on the test set (*test-dev2017*) for comparing with other methods. (b) Cityscapes has 2975 images, 500 images, and 1525 images for training, validation, and test, respectively. For instance segmentation task, Cityscapes has 8 instance categories. (c) LVIS is a recently proposed dataset with the same images as COCO but has more than 1K categories.

¹One deconvolution layer with 2×2 kernel size, one ReLU layer, and one 1×1 convolution layer.

The annotations quality of Cityscapes and LVIS are much higher than COCO, especially on the boundary.

Metrics: For these three datasets, we use the standard mask AP, the average precision over different IoU thresholds (from 0.5 to 0.95) as the primary metric. To better evaluate the boundary quality of the instance segmentation results, we use the newly proposed boundary AP [14] further in some experiments.

Implementation details: We use the PyTorch library [52] and Detectron2 [67] to implement all the models. We use the ResNet-50 pre-trained on ImageNet [56] with FPN [42] as the backbone network, unless otherwise stated. All models are trained using 8 GPUs with stochastic gradient descent (SGD). Momentum and weight decay are set as 0.9 and 0.0001, respectively. For the COCO dataset, the training images are resized to a shorter side from 640 to 800 with a step of 32 pixels and their longer side less or equal to 1333. At inference time, images are resized to the short side of 800 pixels. In the ablation study, all models are trained for 90k iterations. The learning rate is initialized to 0.02 and reduced by a factor of 10 at iteration 60k and 80k. We use a mini-batch of 16 images (2 images per GPU). For the Cityscapes dataset, we use a mini-batch of 8 images (1 image per GPU). All models are trained on the training set for 24k iterations with the learning rate initialized to 0.01, then reduced to 0.001 at iteration 18k and tested on the validation set. At training time, images are resized randomly to a shorter edge from 800 to 1024 pixels with a step of 32 pixels, and their longer edge is less or equal to 2048 pixels. At inference time, images are resized to the shorted edge of 1024 pixels. For the LVIS dataset, we use LVIS*_{v0.5} version. Following [38], the LVIS*_{v0.5} dataset is constructed by keeping only the 80 COCO categories from LVIS_{v0.5}. All models are trained on COCO *train2017* set with standard 1x schedule [67] and tested on the validation set of LVIS*_{v0.5} where images are resized to the short edge of 800 pixels.

4.1.1 Ablation studies.

Each branch in BSM: We first verify the effectiveness of each branch of BSM using Mask R-CNN [27] as the baseline in Tab. 1(a). After adding boundary branch, contraction branch, and expansion branch separately, AP is improved by 0.8, 0.6 and 0.9, respectively. These results prove the effectiveness of each branch. Adding both contraction branch and expansion branch leads to 1.3 AP gain, which means these two branches can complement each other. Adding all three branches results in 1.7 AP gain, which indicates the effectiveness of using boundary supervision explicitly.

Loss function design of contraction and expansion branch: Then we explore the choices of loss function on contraction and expansion branch in Tab. 1(b). Using Binary Cross-Entropy (BCE), weighted Binary Cross-Entropy (weighted BCE), Dice Loss [49] severally, the final AP is 36.2, 36.6, 36.9, respectively. The latter two achieve better performance since they can better handle the class imbalance problems. After combining Dice Loss with BCE or weighted BCE, there are slight performance drops, partially because cross-entropy loss focuses more on pixel-level difference [20] while contraction and expansion branch need to concentrate more on the similarity of two sets of image pixels. So we use Dice Loss as the loss function for contraction and expansion branches.

Low-level RoI features: We present an ablation study on the importance of adding low-level RoI features F'_{RoI} . Low-level features

(a) Effect of each branch in BSM.

Boundary	Contraction	Expansion	AP	AP ₅₀	AP ₇₅
-	-	-	35.2	56.2	37.6
✓	-	-	36.0	56.4	38.7
-	✓	-	35.8	56.6	38.4
-	-	✓	36.1	56.8	38.8
-	✓	✓	36.5	56.8	39.2
✓	✓	✓	36.9	57.2	39.9

(b) Loss function of contraction and expansion branches

BCE	Weighted BCE	Dice	AP	AP ₅₀	AP ₇₅
✓	-	-	36.2	56.5	38.9
-	✓	-	36.6	57.1	39.6
-	-	✓	36.9	57.2	39.9
✓	-	✓	36.6	57.2	39.6
-	✓	✓	36.5	56.8	39.4

(c) Effectiveness of adding low-level RoI features

C2 RoI features	AP	AP ₅₀	AP ₇₅
w/o	36.5	56.8	39.3
w	36.9	57.2	39.9

(d) Ablation of feature information fusion

Add Mask feature	Boudary2Mask conv	AP	AP ₅₀	AP ₇₅
-	-	36.0	56.7	38.6
✓	-	36.6	57.0	39.0
-	✓	36.4	56.5	39.5
✓	✓	36.9	57.2	39.9

Table 1: Ablation studies. We first verify the effectiveness of each branch of our model in (a). Then (b) provides some experiments with different loss functions of contraction and expansion branch. After that, we explore the influence of low-level RoI features in (c), and investigate the impact of information fusion of different branches in (d). All models are tested on COCO *val2017*.

can provide detailed positional information to improve the segmentation quality proven in previous work [11]. We expect this conclusion can apply to our method as well. As shown in Tab. 1(c), using low-level RoI features can contribute to 0.4 AP gain.

Information fusion among different features: We further investigate the effectiveness of information fusion among different branches’ features. Tab. 1(d) offers some results of this aspect: adding mask features to the boundary branch in a residual connection manner results in 0.6 AP gain, which indicates this process can produce better feature representation for boundary prediction. Since there is some information gap between the final boundary feature and mask feature, we add one 1×1 convolution layer when merging boundary features to mask features, and this process leads to 0.4 AP gain. After using the above two operations, our model gains 0.9 AP.

(a) Comparison of different feature deformation methods

Method	AP	Inference Time
w/o fusion	36.0	52ms
w DGMN [76]	36.6	60ms
w DCNV2 [80]	36.8	62ms
w ours	36.9	54ms

Table 2: More analysis studies. (a) offers the results using different feature deformation methods. (b) is used to show the generality of our method where R means ResNet and X means ResNeXt [70]. All results are reported on COCO *val2017*. Inference times are tested using one V100 GPU with single scale testing.

Different feature deformation methods: In our implementation, we use feature warping to generate contraction feature and expansion feature. We also compared some other similar methods to produce these features and provide results in Tab. 2(a). Our baseline model does not use any feature deformation method where the AP is 36.0. After using DGMN [76], we find 0.6 AP gain with an extra 8ms inference time. DCNV2 [80] and our feature warping method achieve a similar performance (36.8 and 36.9), but DCNV2

Method	Inference Time	AP ^{mask}	AP ^{boundary}
Mask R-CNN [27]	48ms	35.2	21.3
PointRend [38]	73ms	36.2	23.3
BMask R-CNN [15]	58ms	36.6	23.4
B2Inst-BlendMask [36]	103ms	36.7	-
BSM	54ms	36.9	23.6

Table 3: Comparison results with baseline and related methods on COCO *val2017*. All the models are trained and tested using the same setting for fair comparison.

uses more inference time. So we choose the flow-based warping in our implementation.

Different backbone networks: In addition to ResNet50, we carry out experiments on other backbone networks, including ResNet101 and ResNeXt101 [70] in Tab. 2(b). With the ResNet101 backbone, our method results in a gain over the baseline of 1.5 AP. We find 1.6 AP gain of our approach on the ResNeXt101 backbone. These decent results prove the generality of our method.

Efficiency and Effectiveness: Both accuracy and efficiency are important factors to consider in practical use. We further compare the inference time, mask AP (AP^{mask}), and recently proposed boundary AP (AP^{boundary}) [14] of our method with baseline Mask R-CNN and other related works including, PointRend [38], BMask R-CNN [15], and B2Inst-BlendMask [36]. Compared with AP^{mask}, AP^{boundary} can better evaluate the accuracy of the boundary. All models use ResNet50 as backbone and use the same inference setting except B2Inst-BlendMask². Results are shown in Tab. 3. Our method has the fastest inference speed among related methods and outperforms other works on AP^{mask} and AP^{boundary}.

4.1.2 Main Results.

Comparison with state-of-the-art methods on COCO: We compare BSM to the state-of-the-art instance segmentation methods on COCO *test-dev2017* in Tab. 4. BSM uses $3 \times$ learning rate schedule with ResNet101 as the backbone network achieves 40.4 AP, which is much better than other state-of-the-art methods. When using cascade architecture, BSM also conducts state-of-the-art results.

²Since the authors of B2Inst do not release their codes and models, all results of B2Inst-BlendMask come from the B2Inst paper.

Method	Backbone	Aug.	Sched.	AP	AP ₅₀	AP ₇₅	AP _S	AP _M	AP _L
Mask R-CNN* [27]	R-50-FPN		1×	35.1	56.4	37.5	18.9	37.0	46.1
CondInst [60]	R-50-FPN		1×	35.4	56.4	37.6	18.4	37.9	46.9
BSM	R-50-FPN		1×	36.5	57.0	39.3	19.4	38.6	47.8
TensorMask [12]	R-50-FPN	✓	6×	35.4	57.2	37.3	16.3	36.8	49.3
BMask R-CNN* [15]	R-50-FPN	✓	1×	36.7	57.0	39.4	17.8	39.1	49.6
CondInst [60]	R-50-FPN	✓	1×	35.9	56.9	38.3	19.1	38.6	46.8
Mask R-CNN* [27]	R-50-FPN	✓	3×	37.3	58.9	40.1	21.1	39.3	47.8
BSM	R-50-FPN	✓	1×	37.0	57.6	40.0	20.5	39.2	47.9
BSM	R-50-FPN	✓	3×	38.9	60.0	42.1	22.0	41.1	49.8
Mask R-CNN [27]	R-101-FPN	✓	3×	38.8	60.9	41.9	21.8	41.4	50.5
MS R-CNN [31]	R-101-FPN		18e	38.3	58.8	41.5	17.8	40.4	54.4
BMask R-CNN* [15]	R-101-FPN	✓	1×	38.0	59.6	40.9	18.1	40.2	54.8
YOLACT-700 [3]	R-101-FPN	✓	4.5×	31.2	50.6	32.8	12.1	33.3	47.1
SipMask [5]	R-101-FPN	✓	6×	38.1	60.2	40.8	17.8	40.8	54.3
BlendMask [6]	R101-FPN	✓	3×	38.4	60.7	41.3	18.2	41.5	53.3
CondInst [60]	R-101-FPN	✓	3×	39.1	60.9	42.0	21.5	41.7	50.9
SOLOv2 [64]	R-101-FPN	✓	3×	39.7	61.8	43.1	21.0	42.2	53.5
BSM	R-101-FPN	✓	1×	38.6	59.6	41.8	21.3	41.2	49.8
BSM	R-101-FPN	✓	3×	40.4	61.9	43.8	22.8	43.0	52.4
BSM	X-101-FPN	✓	3×	41.6	63.7	45.1	24.4	44.4	53.4
Cascade Mask R-CNN*	R50-FPN	✓	1×	36.4	56.9	39.2	17.5	38.7	52.5
Cascade BMask R-CNN	R-50-FPN	✓	1×	37.5	57.3	40.7	17.5	39.8	55.1
Cascade BSM	R-50-FPN	✓	1×	37.9	58.0	41.2	20.7	39.7	51.5
Cascade BSM	R-101-FPN	✓	3×	41.0	62.0	44.6	23.3	41.1	54.0

Table 4: Comparisons with state-of-the-art methods on COCO *test-dev2017*. All models are trained on COCO *train2017*. Aug. means using multi-scale training data augmentation. Sched. means learning rate schedule during training. 1× is 90K iterations, 2× is 180K iterations, 3× is 270K iterations and so on, 18e means 18 epochs. R means ResNet and X means ResNext [70]. * means our implementation.

Method	Backbone	AP	AP ₅₀	AP*	AP* ₅₀
Mask R-CNN [27]	R-50-FPN	33.0	50.0	37.4	58.9
PointRend [38]	R-50-FPN	35.1	62.6	39.3	59.7
BMask R-CNN [15]	R-50-FPN	35.7	61.9	39.2	59.5
BSM	R-50-FPN	36.1	63.0	39.7	60.2
Mask R-CNN [27]	R-101-FPN	33.6	61.8	39.6	61.2
PointRend [38]	R-101-FPN	35.8	63.5	41.5	62.1
BMask R-CNN [15]	R-101-FPN	36.3	62.7	41.2	61.9
BSM	R-101-FPN	36.9	63.5	41.9	62.4

Table 5: Experiments results of BSM and another three methods on Cityscapes and LVIS datasets. AP and AP₅₀ are reported on the validation set of Cityscapes, while AP* and AP*₅₀ are reported on the validation set of LVIS* v0.5.

Visual results comparison: We also provide some visual results on COCO datasets in Fig. 6. Our model can generate better segmentation results than Mask R-CNN and PointRend. PointRend focuses on refining the segmentation results around boundary pixels. BSM can segment instances well in three challenging situations: (a) the appearance of instances is very similar to its surrounding background, (b) complicated scenes, (c) instances overlapping. We argue that the reason why our model can produce better segmentation results than the other two methods is that our method can generate accurate boundaries. And these precise boundaries can help locate instances and distinguish different instances well.

Results on Cityscapes and LVIS datasets: Besides the COCO dataset, we also verify the effectiveness and generalization of BSM on Cityscape [16] and LVIS [25] datasets. The annotations of both datasets have significantly higher quality. We compare our method

with the baseline model Mask R-CNN [27] and another two recent methods, including PointRend [38] and BMask R-CNN [15]. Tab. 5 shows the results on both datasets. Our BSM achieves the best results with ResNet-50 or ResNet-101 as the backbone network on both datasets.

4.2 Experiment: Semantic Segmentation

Overview We also carry out experiments on semantic segmentation task to verify the generality of our BSM. We report results based on DeeplabV3+ [11].

Dataset: (a) Cityscapes semantic segmentation set [16], compared with Cityscapes instance segmentation set introduced in Sec. 4.1, Cityscapes semantic segmentation set has 19 categories. Both datasets have the same training, validation and test images. **(b) BDD [72]** is a recent proposed road scene dataset with 10000 images in total. For dataset split, 7000, 1000, and 2000 images are used for train, validation and test, respectively. For both datasets, we train our models on their training set and report results on validation set.

Metrics: In semantic segmentation, mean IoU (mIoU) is the most commonly used metric. Besides, to evaluate the segmentation quality on boundary, we also report F-score on boundary [54, 59] with four thresholds.

Implementation details: We use the DeeplabV3+ [11] as the baseline model and add our approach to it. Following the original paper, the output stride of backbone network is set to 8. We use the same training and testing setting for different methods (details are in the supplementary) for fair comparison. The architecture of BSM is the

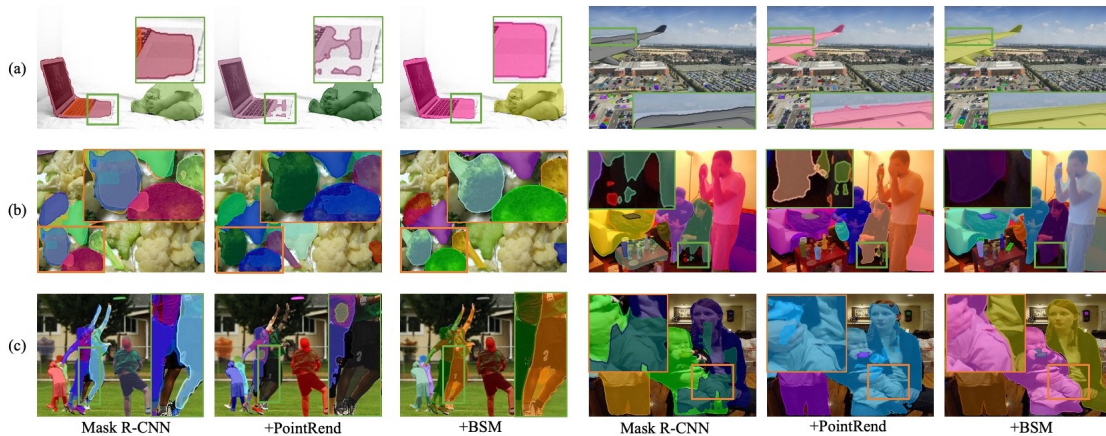


Figure 6: Visualization and comparison results of Mask R-CNN [27], PointRend [38] and our BSM on the COCO *val2017* using ResNet-50 [29] with FPN [42] as backbone. Compared with the other two methods, BSM can produce better segmentation results. Best viewed on screen and zoom in.

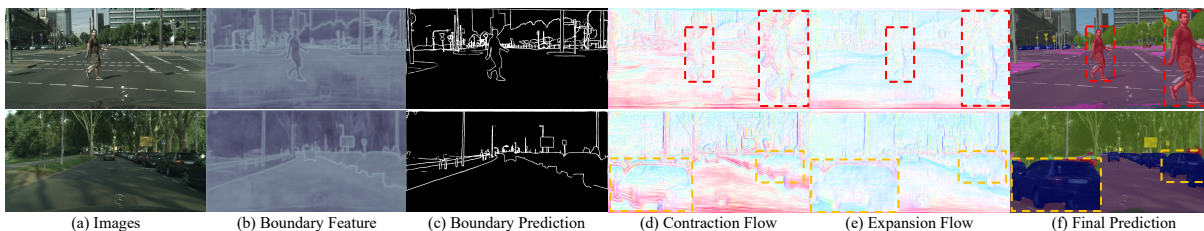


Figure 7: Visualization of our BSM using DeeplabV3+ as baseline on Cityscapes. From left to right, (a) is the original image, we visualize the boundary feature in (b) and boundary prediction in (c), also two opposite flow field in (d) and (e) respectively. The final mask prediction is shown in (f). Best view it in color and zoom in.

same as that for instance segmentation. We use the res2 features as low-level features to provide detailed location information.

Main Results Quantitatively, we compare BSM with DeeplabV3+ and PointRend in Tab. 6. For Cityscapes dataset, with ResNet50 and ResNet101 as backbone network, our method obtains 1.0 and 1.1 mIoU gain over PointRend. With the reduction of F-score threshold, our method achieves a larger performance gain, which means our model can generate more precise boundaries. For BDD dataset, our BSM obtains consistent performance improvements as well.

Visual Results In Fig. 7, we give the visualization on semantic segmentation task. As shown in Fig. 7(b) and (c), we observe the clear and thin boundary feature and boundary prediction. The two opposite flow fields, are shown in Fig. 7 (d) and (e). Final results are shown in Fig. 7(f). Besides, as shown in the right part of Fig. 2, BSM has better visual results than PointRend on two different types of objects: things and scenes. Both visual examples prove our motivation: boundary squeezing process can generate more accurate boundary via learned flow field warping and improve segmentation result.

5 CONCLUSION

In this paper, we propose a conceptually new idea to model the segmentation process as boundary squeezing. We design the opposite flow-based modules named Boundary Squeeze Module (BSM).

Method	backbone	dataset	mIoU \uparrow	F1(12px) \uparrow	F1(9px) \uparrow	F1(5px) \uparrow	F1(3px) \uparrow
DeeplabV3+ [11]	R-50	Cityscapes	77.9	78.3	77.0	72.9	62.3
+PointRend [78]	R-50	Cityscapes	78.5	79.6	78.5	74.8	64.1
+BSM	R-50	Cityscapes	79.5	80.9	79.7	76.4	67.7
DeeplabV3+ [11]	R-101	Cityscapes	78.9	79.9	78.2	72.8	62.5
+PointRend [78]	R-101	Cityscapes	79.5	80.7	78.6	74.8	64.6
+BSM	R-101	Cityscapes	80.6	82.9	81.8	78.7	69.9
DeeplabV3+ [11]	R-50	BDD	61.2	76.6	75.4	70.8	61.6
+PointRend [78]	R-50	BDD	62.3	79.1	77.3	72.6	63.9
+BSM	R-50	BDD	63.5	81.1	79.9	76.2	67.9

Table 6: Comparison results of DeeplabV3+, PointRend and BSM. All results are reported on the validation set. X-px means X pixels along the boundaries. All the models are trained in the same setting.

The supervisions of BSM can be obtained via dilation operator, erosion operator of the existing annotations. The boundary squeezing process can be achieved via flow-based warping. After BSM, the feature contains precise boundary information, and the mask quality is much better. We verify our proposed BSM on two different tasks, including instance segmentation and semantic segmentation. Extensive results prove that our BSM outperforms previous work PointRend in various settings. We also show significant gains over various baselines on both COCO and Cityscapes datasets. One shortcoming of BoundarySqueeze is the limited resolution problem which will be our future work.

REFERENCES

- [1] Gedas Bertasius, Jianbo Shi, and Lorenzo Torresani. 2016. Semantic Segmentation With Boundary Neural Fields. In *CVPR*.
- [2] Gedas Bertasius, Lorenzo Torresani, Stella X. Yu, and Jianbo Shi. 2017. Convolutional Random Walk Networks for Semantic Image Segmentation. In *CVPR*.
- [3] Daniel Bolya, Chong Zhou, Fanyi Xiao, and Yong Jae Lee. 2019. YOLACT: Real-time Instance Segmentation. In *ICCV*.
- [4] Zhaowei Cai and Nuno Vasconcelos. 2018. Cascade R-CNN: Delving Into High Quality Object Detection. In *CVPR*.
- [5] Jiale Cao, Rao Muhammad Anwer, Hisham Cholakkal, Fahad Shahbaz Khan, Yanwei Pang, and Ling Shao. 2020. SipMask: Spatial Information Preservation for Fast Image and Video Instance Segmentation. *arXiv preprint arXiv:2007.14772* (2020).
- [6] Hao Chen, Kunyang Sun, Zhi Tian, Chunhua Shen, Yongming Huang, and Youliang Yan. 2020. BlendMask: Top-Down Meets Bottom-Up for Instance Segmentation. In *CVPR*.
- [7] Kai Chen, Jiangmiao Pang, Jiaqi Wang, Yu Xiong, Xiaoxiao Li, Shuyang Sun, Wansen Feng, Ziwei Liu, Jianping Shi, Wanli Ouyang, Chen Change Loy, and Dahua Lin. 2019. Hybrid task cascade for instance segmentation. In *CVPR*.
- [8] Liang-Chieh Chen, Jonathan T. Barron, George Papandreou, Kevin Murphy, and Alan L. Yuille. 2016. Semantic Image Segmentation With Task-Specific Edge Detection Using CNNs and a Discriminatively Trained Domain Transform. In *CVPR*.
- [9] Liang-Chieh Chen, George Papandreou, Iasonas Kokkinos, Kevin Murphy, and Alan L. Yuille. 2018. DeepLab: Semantic Image Segmentation with Deep Convolutional Nets, Atrous Convolution, and Fully Connected CRFs. *PAMI* (2018).
- [10] Liang-Chieh Chen, George Papandreou, Florian Schroff, and Hartwig Adam. 2017. Rethinking Atrous Convolution for Semantic Image Segmentation. *arXiv preprint* (2017).
- [11] Liang-Chieh Chen, Yukun Zhu, George Papandreou, Florian Schroff, and Hartwig Adam. 2018. Encoder-Decoder with Atrous Separable Convolution for Semantic Image Segmentation. In *ECCV*.
- [12] Xinlei Chen, Ross Girshick, Kaiming He, and Piotr Dollár. 2019. Tensormask: A foundation for dense object segmentation. In *ICCV*.
- [13] Xier Chen, Yanchao Lian, Licheng Jiao, Haoran Wang, Yanjie Gao, and Shi Lingling. 2020. Supervised Edge Attention Network for Accurate Image Instance Segmentation. In *ECCV*.
- [14] Bowen Cheng, Ross Girshick, Piotr Dollár, Alexander C. Berg, and Alexander Kirillov. 2021. Boundary IoU: Improving Object-Centric Image Segmentation Evaluation. In *CVPR*.
- [15] Tianheng Cheng, Xinggang Wang, Lichao Huang, and Wenyu Liu. 2020. Boundary-preserving Mask R-CNN. In *ECCV*.
- [16] Marius Cordts, Mohamed Omran, Sebastian Ramos, Timo Rehfeld, Markus Enzweiler, Rodrigo Benenson, Uwe Franke, Stefan Roth, and Bernt Schiele. 2016. The Cityscapes Dataset for Semantic Urban Scene Understanding. In *CVPR*.
- [17] Jifeng Dai, Kaiming He, Yi Li, Shaoqing Ren, and Jian Sun. 2016. Instance-sensitive fully convolutional networks. In *ECCV*. Springer.
- [18] Jifeng Dai, Haozhi Qi, Yuwen Xiong, Yi Li, Guodong Zhang, Han Hu, and Yichen Wei. 2017. Deformable Convolutional Networks. In *ICCV*.
- [19] Bert De Brabandere, Davy Neven, and Luc Van Gool. 2017. Semantic instance segmentation with a discriminative loss function. *arXiv preprint arXiv:1708.02551* (2017).
- [20] Ruoxi Deng, Chunhua Shen, Shengjun Liu, Huibing Wang, and Xinru Liu. 2018. Learning to predict crisp boundaries. In *ECCV*.
- [21] Alexey Dosovitskiy, Philipp Fischer, Eddy Ilg, Philip Hausser, Caner Hazirbas, Vladimir Golkov, Patrick Van Der Smagt, Daniel Cremers, and Thomas Brox. 2015. FlowNet: Learning optical flow with convolutional networks. In *CVPR*.
- [22] Adrian N Evans and Xin U Liu. 2006. A morphological gradient approach to color edge detection. *TIP* (2006).
- [23] Jun Fu, Jing Liu, Haijie Tian, Zhiwei Fang, and Hanqing Lu. 2019. Dual attention network for scene segmentation. In *CVPR*.
- [24] Ke Gong, Xiaodan Liang, Yicheng Li, Yimin Chen, Ming Yang, and Liang Lin. 2018. Instance-level Human Parsing via Part Grouping Network. In *ECCV*.
- [25] Agrim Gupta, Piotr Dollár, and Ross Girshick. 2019. LVIS: A dataset for large vocabulary instance segmentation. In *ICCV*. 5356–5364.
- [26] Bharath Hariharan, Pablo Arbeláez, Ross Girshick, and Jitendra Malik. 2014. Simultaneous detection and segmentation. In *ECCV*. Springer.
- [27] Kaiming He, Georgia Gkioxari, Piotr Dollár, and Ross Girshick. 2017. Mask R-CNN. In *ICCV*.
- [28] Kaiming He, Xiangyu Zhang, Shaoqing Ren, and Jian Sun. 2015. Delving Deep into Rectifiers: Surpassing Human-Level Performance on ImageNet Classification. In *ICCV*.
- [29] Kaiming He, Xiangyu Zhang, Shaoqing Ren, and Jian Sun. 2016. Deep Residual Learning for Image Recognition. In *CVPR*.
- [30] Zhaojin Huang, Lichao Huang, Yongchao Gong, Chang Huang, and Xinggang Wang. 2019. Mask Scoring R-CNN. In *CVPR*.
- [31] Zhaojin Huang, Lichao Huang, Yongchao Gong, Chang Huang, and Xinggang Wang. 2019. Mask scoring r-cnn. In *Proceedings of the IEEE/CVF Conference on Computer Vision and Pattern Recognition*. 6409–6418.
- [32] Zilong Huang, Xinggang Wang, Lichao Huang, Chang Huang, Yunchao Wei, and Wenyu Liu. 2019. Ccnet: Criss-cross attention for semantic segmentation. In *ICCV*.
- [33] Max Jaderberg, Karen Simonyan, Andrew Zisserman, and Koray Kavukcuoglu. 2015. Spatial Transformer Networks. In *NeurIPS*.
- [34] Michael Kass, Andrew Witkin, and Demetri Terzopoulos. 1988. Snakes: Active contour models. *International journal of computer vision* 1, 4 (1988), 321–331.
- [35] Tsung-Wei Ke, Jyh-Jing Hwang, Ziwei Liu, and Stella X. Yu. 2018. Adaptive Affinity Fields for Semantic Segmentation. In *ECCV*.
- [36] Myungchul Kim, Sanghyun Woo, Dahun Kim, and In So Kweon. 2021. The devil is in the boundary: Exploiting boundary representation for basis-based instance segmentation. In *Proceedings of the IEEE/CVF Winter Conference on Applications of Computer Vision*. 929–938.
- [37] Alexander Kirillov, Evgeny Levinkov, Bjoern Andres, Bogdan Savchynskyy, and Carsten Rother. 2017. Instancecut: from edges to instances with multicut. In *CVPR*. 5008–5017.
- [38] Alexander Kirillov, Yuxin Wu, Kaiming He, and Ross Girshick. 2020. Pointrend: Image segmentation as rendering. In *CVPR*.
- [39] Iasonas Kokkinos. 2015. Pushing the boundaries of boundary detection using deep learning. *arXiv preprint arXiv:1511.07386* (2015).
- [40] Xiangtai Li, Xia Li, Li Zhang, Cheng Guangliang, Jianping Shi, Zhouchen Lin, Yunhai Tong, and Shaohua Tan. 2020. Improving Semantic Segmentation via Decoupled Body and Edge Supervision. In *ECCV*.
- [41] Xia Li, Zhisheng Zhong, Jianlong Wu, Yibo Yang, Zhouchen Lin, and Hong Liu. 2019. Expectation-Maximization Attention Networks for Semantic Segmentation. In *ICCV*.
- [42] Tsung-Yi Lin, Piotr Dollár, Ross B. Girshick, Kaiming He, Bharath Hariharan, and Serge J. Belongie. 2017. Feature Pyramid Networks for Object Detection. In *CVPR*.
- [43] Tsung-Yi Lin, Priya Goyal, Ross Girshick, Kaiming He, and Piotr Dollár. 2018. Focal loss for dense object detection. *PAMI* (2018).
- [44] Tsung-Yi Lin, Michael Maire, Serge Belongie, James Hays, Pietro Perona, Deva Ramanan, Piotr Dollár, and C Lawrence Zitnick. 2014. Microsoft coco: Common objects in context. In *ECCV*.
- [45] Shu Liu, Lu Qi, Haifang Qin, Jianping Shi, and Jiaya Jia. 2018. Path aggregation network for instance segmentation. In *CVPR*.
- [46] Yiding Liu, Siyu Yang, Bin Li, Wengang Zhou, Jizheng Xu, Houqiang Li, and Yan Lu. 2018. Affinity derivation and graph merge for instance segmentation. In *ECCV*.
- [47] Jonathan Long, Evan Shelhamer, and Trevor Darrell. 2015. Fully convolutional networks for semantic segmentation. In *CVPR*.
- [48] Kevis-Kokitsi Maninis, Jordi Pont-Tuset, Pablo Arbeláez, and Luc Van Gool. 2017. Convolutional oriented boundaries: From image segmentation to high-level tasks. *PAMI* (2017).
- [49] Fausto Milletari, Nassir Navab, and Seyed-Ahmad Ahmadi. 2016. V-net: Fully convolutional neural networks for volumetric medical image segmentation. In *3DV*. IEEE.
- [50] Davy Neven, Bert De Brabandere, Marc Proesmans, and Luc Van Gool. 2019. Instance segmentation by jointly optimizing spatial embeddings and clustering bandwidth. In *CVPR*.
- [51] Giuseppe Papari and Nicolai Petkov. 2011. Edge and line oriented contour detection: State of the art. *IMAGE VISION COMPUT* (2011).
- [52] Adam Paszke, Sam Gross, Francisco Massa, Adam Lerer, James Bradbury, Gregory Chanan, Trevor Killeen, Zeming Lin, Natalia Gimelshein, Luca Antiga, et al. 2019. Pytorch: An imperative style, high-performance deep learning library. In *Advances in neural information processing systems*.
- [53] Sida Peng, Wen Jiang, Huaijin Pi, Xiuli Li, Hujun Bao, and Xiaowei Zhou. 2020. Deep Snake for Real-Time Instance Segmentation. In *CVPR*.
- [54] Federico Perazzi, Jordi Pont-Tuset, Brian McWilliams, Luc Van Gool, Markus Gross, and Alexander Sorkine-Hornung. 2016. A Benchmark Dataset and Evaluation Methodology for Video Object Segmentation. In *CVPR*.
- [55] Shaoqing Ren, Kaiming He, Ross Girshick, and Jian Sun. 2015. Faster r-cnn: Towards real-time object detection with region proposal networks. In *NeurIPS*.
- [56] Olga Russakovsky, Jia Deng, Hao Su, Jonathan Krause, Sanjeev Satheesh, Sean Ma, Zhiheng Huang, Andrej Karpathy, Aditya Khosla, Michael Bernstein, Alexander C. Berg, and Li Fei-Fei. 2015. ImageNet Large Scale Visual Recognition Challenge. *IJCV* (2015).
- [57] Wei Shen, Xinggang Wang, Yan Wang, Xiang Bai, and Zhijiang Zhang. 2015. Deepcontour: A deep convolutional feature learned by positive-sharing loss for contour detection. In *CVPR*.
- [58] Jingkuan Song, Zhilong Zhou, Lianli Gao, Xing Xu, and Heng Tao Shen. 2018. Cumulative nets for edge detection. In *Proceedings of the 26th ACM international conference on Multimedia*. 1847–1855.
- [59] Towaki Takikawa, David Acuna, Varun Jampani, and Sanja Fidler. 2019. Gated-SCNN: Gated Shape CNNs for Semantic Segmentation. *ICCV* (2019).

- [60] Zhi Tian, Chunhua Shen, and Hao Chen. 2020. Conditional Convolutions for Instance Segmentation. In *ECCV*.
- [61] Thang Vu, Kang Haeyong, and Chang D Yoo. 2021. SCNet: Training Inference Sample Consistency for Instance Segmentation. In *AAAI*.
- [62] Xialong Wang, Ross Girshick, Abhinav Gupta, and Kaiming He. 2018. Non-Local Neural Networks. In *CVPR*.
- [63] Xinlong Wang, Tao Kong, Chunhua Shen, Yuning Jiang, and Lei Li. 2020. SOLO: Segmenting Objects by Locations. In *ECCV*.
- [64] Xinlong Wang, Rufeng Zhang, Tao Kong, Lei Li, and Chunhua Shen. 2020. SOLOv2: Dynamic and Fast Instance Segmentation. In *NeurIPS*.
- [65] Svante Wold, Kim Esbensen, and Paul Geladi. 1987. Principal component analysis. *Chemom. Intell. Lab. Syst.* (1987).
- [66] Jialian Wu, Liangchen Song, Tiancai Wang, Qian Zhang, and Junsong Yuan. 2020. Forest r-cnn: Large-vocabulary long-tailed object detection and instance segmentation. In *Proceedings of the 28th ACM International Conference on Multimedia*. 1570–1578.
- [67] Yuxin Wu, Alexander Kirillov, Francisco Massa, Wan-Yen Lo, and Ross Girshick. 2019. Detectron2. <https://github.com/facebookresearch/detectron2>.
- [68] Tete Xiao, Yingcheng Liu, Bolei Zhou, Yuning Jiang, and Jian Sun. 2018. Unified Perceptual Parsing for Scene Understanding. In *ECCV*.
- [69] Enze Xie, Peize Sun, Xiaoge Song, Wenhai Wang, Xuebo Liu, Ding Liang, Chunhua Shen, and Ping Luo. 2019. PolarMask: Single Shot Instance Segmentation with Polar Representation. *arXiv preprint arXiv:1909.13226* (2019).
- [70] Saining Xie, Ross Girshick, Piotr Dollár, Zhuowen Tu, and Kaiming He. 2017. Aggregated residual transformations for deep neural networks. In *Proceedings of the IEEE conference on computer vision and pattern recognition*. 1492–1500.
- [71] Saining Xie and Zhuowen Tu. 2015. Holistically-nested edge detection. In *ICCV*.
- [72] Fisher Yu, Haofeng Chen, Xin Wang, Wenqi Xian, Yingying Chen, Fangchen Liu, Vashisht Madhavan, and Trevor Darrell. 2020. BDD100K: A diverse driving dataset for heterogeneous multitask learning. In *CVPR*.
- [73] Fisher Yu and Vladlen Koltun. 2016. Multi-Scale Context Aggregation by Dilated Convolutions. *ICLR* (2016).
- [74] Zhiding Yu, Chen Feng, Ming-Yu Liu, and Srikumar Ramalingam. 2017. Casenet: Deep category-aware semantic edge detection. In *CVPR*.
- [75] Yuhui Yuan, Xilin Chen, and Jingdong Wang. 2020. Object-contextual representations for semantic segmentation. *ECCV* (2020).
- [76] Li Zhang, Dan Xu, Anurag Arnab, and Philip H.S. Torr. 2020. Dynamic Graph Message Passing Networks. In *CVPR*.
- [77] Rufeng Zhang, Zhi Tian, Chunhua Shen, Mingyu You, and Youliang Yan. 2020. Mask Encoding for Single Shot Instance Segmentation. In *CVPR*.
- [78] Hengshuang Zhao, Jianping Shi, Xiaojuan Qi, Xiaogang Wang, and Jiaya Jia. 2017. Pyramid Scene Parsing Network. In *CVPR*.
- [79] Bolei Zhou, Hang Zhao, Xavier Puig, Tete Xiao, Sanja Fidler, Adela Barriuso, and Antonio Torralba. [n.d.]. Semantic understanding of scenes through the ade20k dataset. *IJCV* ([n. d.]).
- [80] Xizhou Zhu, Han Hu, Stephen Lin, and Jifeng Dai. 2019. Deformable convnets v2: More deformable, better results. In *CVPR*. 9308–9316.
- [81] Xizhou Zhu, Yuwen Xiong, Jifeng Dai, Lu Yuan, and Yichen Wei. 2017. Deep Feature Flow for Video Recognition. In *CVPR*.
- [82] Yi Zhu, Karan Sapra, Fitsum A. Reda, Kevin J. Shih, Shawn Newsam, Andrew Tao, and Bryan Catanzaro. 2019. Improving Semantic Segmentation via Video Propagation and Label Relaxation. In *CVPR*.